ANALYTICAL SCIENCES FEBRUARY 2010, VOL. 26

Reviews

Determination of Surface Composition by X-ray Photoelectron Spectroscopy Taking into Account Elastic Photoelectron Collisions

Aleksander JABLONSKI

Institute of Physical Chemistry, Polish Academy of Sciences, ul. Kasprzaka 44/52, 01-224 Warsaw, Poland

It is now well known that elastic photoelectron scattering in the surface region of solids cannot be ignored in the mathematical formalism of quantitative XPS. Elastic collisions may increase or decrease the photoelectron signal intensity, depending on the experimental configuration. Consequently, it is advisable to take into account these effects in calculations of the surface composition. In certain experimental geometries, the photoelectron intensity is practically unaffected by elastic scattering events (configurations defined by the so-called "Master Angle"), and in principle such geometries should be recommended for measurements. Unfortunately, they usually cannot be implemented in typical constructions of spectrometers. In the present paper, different procedures for estimating corrections for elastic scattering events are overviewed. The influence of these correction procedures has been illustrated on examples of AuAgCu and AuAgPdCu alloys. It turned out that elastic photoelectron collisions substantially decrease the signal intensities selected for analysis. However, they are diminished by roughly the same factor. As a consequence, the calculated surface composition is only slightly modified by the correction procedure. This effect may not be of general validity for all solids, and the algorithms for calculating the surface composition should have an option for including any elastic scattering effects. Further efforts are needed to improve the predictive formulas providing corrections for elastic scattering effects.

(Received July 23, 2009; Accepted November 20, 2009; Published February 10, 2010)

1 Introduction

X-ray photoelectron spectroscopy (XPS) is presently one of the most versatile tools for studies of solid surfaces. Despite the fact that this technique was developed in the second half of 1960s, it is presently used in surface studies with increasing frequency. As indicated in recent work,[1] the number of studies in which this technique is used is steadily growing. Over the last decade, this number has roughly doubled, reaching 5469 in 2007. There are several reasons for the high popularity of the XPS technique. Firstly, it is applicable to a great variety of samples, particularly to nonconductors, in contrast to Auger electron spectroscopy. Secondly, considerable advances in nanotechnology require a tool that makes possible studies of solid surfaces in the nanometer range. Furthermore, we can now observe considerable progress in instrumentation. Spectrometers with a scanning facility are now available, which makes possible the mapping of a particular chemical species at the surface. Finally, the quantification of XPS is considered to be reasonably reliable, since photoelectron emission is a one-electron process that can be described by theory with relatively good accuracy.

Much attention has been devoted to the problem of quantifying XPS. The status of quantification by 1974 had been extensively reviewed by Fadley *et al*.[2] These authors outlined a mathematical formalism associated with this technique, which in fact, after few modifications, has been used until today. An introduction to quantitative XPS can also be found in numerous later reviews[3,4] and monographs.[5,6]

A determination of the surface composition by XPS requires knowledge of a reliable and accurate theoretical model relating the photoelectron signal intensity with the concentration of atoms emitting considered photoelectrons. The commonly used formalism is based on several assumptions specifying the sample and assumptions related to photoelectron transport in

E-mail: jablo@ichf.edu.pl

solids. We assume that the sample is ideally flat, so the emitted photoelectrons are not recaptured by any surface protrusions. Furthermore, it is expected to be amorphous or polycrystalline. Consequently, the observed signal intensities are not modified by diffraction, or forward-focusing. Finally, we expect that the sample composition has a uniform in-depth composition within the sampling depth of XPS. The X-rays are assumed to be attenuated negligibly in the analyzed region. The ionizing radiation is not reflected from the surface, and there are no refraction effects. Two further assumptions conveniently simplify the formalism. The photoelectron intensity is assumed to be attenuated exponentially, and the photoelectron trajectories are expected to be linear from the point of emission up to the sample surface. Certainly, the photoelectron trajectories may deviate from linearity due to elastic interactions with atoms of the solid; the last assumption was considered to be controversial even in early days of electron spectroscopies. In his theoretical analysis of the Auger-plasmon-satellite intensities, Feibelman[7] wrote: "... one should make some effort to account for deflection of escaping electrons by elastic scattering from ion cores". Fadley *et al.*[2] admitted that the influence of elastic electron scattering on the angular distribution of emitted electron is assumed to be negligible, but "... a slight smearing effect ... cannot be ruled out".

The importance of elastic scattering effects in quantitative XPS analysis was initially proved in a series of papers by Baschenko and Nefedov.[8–10] These authors indicated that photoelectron elastic scattering events have a non-negligible effect on the angular distribution of photoemission. Results published by Baschenko and Nefedov stimulated further studies of photoelectron transport in the surface region of solids. Early research, until 1989, was reviewed by Jablonski.[11] Similar reviews were also published more recently.[4,12]

Although presently an important role of elastic photoelectron collisions in quantitative XPS is commonly recognized, it is not a common practice to account for these effects in routine analysis. This problem is extensively discussed in the present work.

2 Theory

We start with a brief introduction to the common formalism of XPS in which elastic photoelectron scattering is neglected. The photoelectron signal intensity, dI_x, originating from a thin layer of thickness dz located at a depth z is given by

$$dI_x = TD_eF_xA\Delta\Omega N(d\sigma_x/d\Omega)\exp[-z/(\lambda_{in}\cos\alpha)]dz, \quad (1)$$

where T is the analyzer transmission function, D_e the detector efficiency, F_x the flux of incident X-rays, A the analyzed area, $\Delta\Omega$ the solid acceptance angle of the analyzer, N the atomic density of a given element (number of atoms in unit volume), α the detection angle with respect to the surface normal, λ_{in} the inelastic mean free path of analyzed photoelectrons (IMFP), and $d\sigma_x/d\Omega_x$ the differential photoelectric cross section. The latter parameter has the following form:

$$d\sigma_x/d\Omega = \sigma_x W(\beta,\psi) = \sigma_x \frac{1}{4\pi}\left[1-\frac{\beta}{4}(3\cos^2\psi-1)\right], \quad (2)$$

where σ_x is the total photoelectric cross section, $W(\beta,\psi)$ the photoelectric cross section normalized to unity, ψ the angle between the direction of X-rays and the direction towards the analyzer, and β the asymmetry parameter.

If the area irradiated by X-rays is larger than the analyzed area, then the following approximate relation holds

$$A = A_0/\cos\alpha, \quad (3)$$

where A_0 is the area seen by the analyzer at the normal direction of analysis. Upon integration of Eq. (1) with respect to depth z, while taking into account Eq. (3), we obtain an expression describing the photoelectron signal intensity from a uniform semi-infinite solid,

$$I_x = TD_eA_0F_x\Delta\Omega N\lambda_{in}(d\sigma_x/d\Omega). \quad (4)$$

The influence of photoelectron elastic collisions on the signal intensity is well described with two correcting factors, Q_x and β_{eff}, both modifying the photoelectron photoelectric cross section[11,13]

$$(d\sigma_x/d\Omega)_{corr} = \sigma_xQ_xW(\beta_{eff},\psi) = \sigma_xQ_x\frac{1}{4\partial}\left[1-\frac{\beta_{eff}}{4}(3\cos^2\psi-1)\right]. \quad (5)$$

Extensive compilations of these parameters are available in the literature.[14] However, these data refer to elemental solids, and thus are of limited use in practical analysis. Corrections Q_x and β_{eff} are also compiled in NIST database 82.[15] Although the NIST data are available for elements and compounds, they cannot be conveniently used in routine calculations of quantitative XPS. Several predictive formulas for Q_x and β_{eff} were proposed[16–19] which, in principle, are applicable to any solid. They originate from two procedures:

1. An analytical solution of the kinetic Boltzmann equation within the so-called transport approximation.[16–18]
2. A fit of analytical expressions to results of Monte Carlo simulations of photoelectron transport in solids.[19]

2·1 Kinetic Boltzmann equation

It has been shown[16] that the photoelectron signal intensity derived within the transport approximation can be described by the following formula:

$$I_x^{el} = Y_x\frac{\mu\omega\lambda_{tr}}{4\pi}\left[(1-\omega)^{-1/2}H(\mu,\omega)-\frac{\beta}{4}(3\cos^2\psi-1)+\frac{\beta\omega}{16}(3\cos^2\theta-1)H(\mu,\omega)\int_0^1\frac{x(H(x,\omega))}{x+\mu}(3x^2-1)dx\right], \quad (6)$$

where θ is the angle between the direction of X-rays and the surface normal, $\mu = \cos\alpha$, λ_{tr}, is the transport mean free path, ω is the single-scattering albedo,

$$\omega = \frac{\lambda_{in}}{\lambda_{in}+\lambda_{tr}}, \quad (7)$$

$H(x, \omega)$ is the Chandrasekhar function,[20] and

$$Y_x = TD_eF_x\Delta\Omega N\lambda_{in}\sigma_x(A_0/\mu). \quad (8)$$

The photoelectron elastic scattering influence on the signal intensity is fully described here by the transport mean free path. This parameter is related to the differential elastic scattering cross section, $d\sigma_e/d\Omega$. For an element, we have

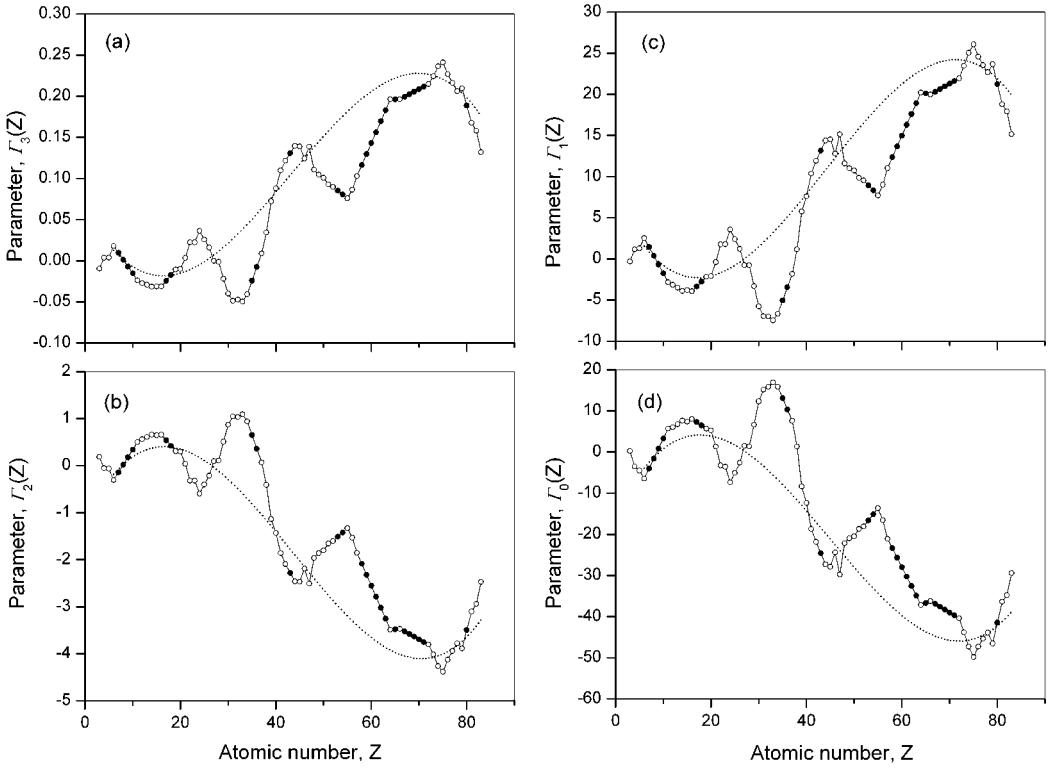

Fig. 1 Atomic number dependence of parameters Γ_k. Open circles, parameters calculated by fitting Eq. (16) to parameters ζ calculated by Jablonski and Powell;[18] filled circles, parameters obtained by interpolation. A solid line is shown here to guide the eye. For a comparison, the atomic number dependence calculated in Ref. 17 is shown as a dotted line. (a) Parameter Γ_3(Z), (b) parameter Γ_2(Z), (c) parameter Γ_1(Z), (d) parameter Γ_0(Z).

$$\lambda_{tr} = \frac{1}{N\sigma_{tr}}, \tag{9}$$

where σ_{tr} is the transport cross section

$$\sigma_{tr} = 2\pi\int_0^{\pi}(1-\cos\vartheta)\frac{d\sigma_e}{d\Omega}\sin\vartheta d\vartheta. \tag{10}$$

Equation (6) can be written in the form

$$I_x^{el} = TD_eA_0F_x\Delta\Omega N\lambda_{in}\sigma_xQ_x\frac{1}{4\pi}\left[1-\frac{\beta_{eff}}{4}(3\cos^2\psi-1)\right], \tag{11}$$

where

$$Q_x = \frac{\lambda_{tr}}{\lambda_{in}+\lambda_{tr}}(D_1+D_2), \tag{12a}$$

$$\beta_{eff} = \frac{\lambda_{tr}}{\lambda_{in}+\lambda_{tr}}\frac{\beta}{Q_x}, \tag{12b}$$

$$D_1 = (1-\omega)^{-1/2}H(\mu,\omega), \tag{12c}$$

$$D_2 = \frac{\beta\omega}{16}(3\cos^2\theta-1)H(\mu,\omega)\int_0^1\frac{xH(x,\omega)}{x+\mu}(3x^2-1)dx. \tag{12d}$$

The term D_2 was found to be considerably smaller than the term D_1 and neglecting the term D_2 affected the correction Q_x by less than 1%.[16] Consequently, Eq. (12a) – (12d) can be written as[16,17]

$$Q_x = (1-\omega)^{1/2}H(\cos\alpha,\omega), \tag{13}$$

$$\beta_{eff} = \frac{(1-\omega)\beta}{Q_x}, \tag{14}$$

$$\omega = \frac{1}{1+\zeta}, \tag{15}$$

where ζ is the ratio of the transport mean free path, λ_{tr}, to the inelastic mean free path, λ_{in}. We can see that the elastic scattering effects in quantitative XPS, within the formalism of the transport approximation, can be fully described by one parameter, ζ. There are different methods for determining this parameter for a given solid from an analytical formalism. They are briefly reviewed below.

2·2 Algorithm of Jablonski

It has been postulated that the dependence of the ratio ζ on the energy for any solid is well described by the following function:[17,18]

$$\zeta = \exp\left[\sum_{k=0}^{3}\Gamma_k(\ln E)^k\right], \tag{16}$$

where Γ_0, Γ_1, Γ_2, and Γ_3 are fitted parameter characteristic for a given solid. This equation is a generalized form of an equation successfully used for describing the energy dependence of the IMFP,[21]

$$\lambda_{in} = cE^p = \exp(p\ln E + \ln c) = \exp(\Gamma_1 \ln E + \Gamma_0). \quad (17)$$

Jablonski[17] calculated the parameters Γ_k for 27 elements and for 22 energies in the range from 50 eV to 2 keV. The IMFPs were taken from Tanuma *et al.*[22] while the TMFPs were calculated for these elements using the relativistic partial wave expansion method (PWEM) under an assumption that the interaction between an electron and an atom of the solid follows the Thomas–Fermi–Dirac potential. It has been found that the dependence of the parameters Γ_k follows roughly a curve that is well approximated by a polynomial,

$$\Gamma_k = \Gamma_k(Z) = a_{k3}Z^3 + a_{k2}Z^2 + a_{k1}Z + a_{k0} = \sum_{n=0}^{3} a_{kn}Z^n. \quad (18)$$

The fitted coefficients, a_{kn}, are available from Table 2 of Ref. 17. The resulting atomic number dependence of parameters Γ_k is shown in Figs. 1(a) – 1(d) as a dotted line. Introducing Eq. (18) into Eq. (16), we obtain a simple equation expressing the ratio ζ:

$$\zeta = \exp\left[\sum_{k=0}^{3}\sum_{n=0}^{3} a_{kn}Z^n(\ln E)^k\right]. \quad (19)$$

From the shape of the curves shown in Figs. 1(a) – 1(d), it follows that the coefficients Γ_k depend predominantly on the atomic number. Thus, we may generalize Eq. (19) to compounds, assuming that the weighted average of the atomic numbers can be introduced into this equation:

$$\overline{Z} = \sum_{i=1}^{m} x_i Z_i, \quad (20)$$

where m is the number of elements present in the sample, and the weight x_i the atom fraction of the ith element.

2·3 Algorithm of Jablonski and Powell

The ratios ζ can be calculated using the coefficients Γ_k of improved accuracy. Jablonski and Powell[18] repeated the above analysis based on an extended set of the IMFPs and the TMFPs. The IMFP values were determined for 57 elements, partly from the optical data (34 elements), and partly from the predictive formula[23] (23 elements). For each element, 53 energies were considered; they were distributed roughly logarithmically in the energy range from 50 eV to 2 keV. For these elements and energies, the TMFP values were calculated from the relativistic PWEM calculations. Thus, in total, the analysis was founded on a set of 3021 ratios ζ. The fit of Eq. (16) to this set provided, in the first step, the parameters Γ_k. They are plotted in Figs. 1(a) – 1(d). The numerical values of these parameters are compiled in Ref. 18 for atomic numbers from $Z = 3$ to 83. We can now see that the dependences of parameters Γ_k on the atomic number are oscillating functions that cannot be approximated accurately by Eq. (18). It has been postulated to use tabulated parameters, Γ_k, in calculations of the ratios ζ rather than to make an attempt to fit this dependence with a more sophisticated function than Eq. (18).

2·4 Algorithms of Seah and Gilmore

Seah and Gilmore[19] derived the predictive expressions for the Q_x and β_{eff} corrections from an extensive database of these parameters obtained by Jablonski[14] from the Monte Carlo simulations of photoelectron transport. The latter data were originally fitted by the following expressions[13,14]

$$\beta_{eff} = a_1\cos^2\alpha + a_2\cos\alpha + a_3, \quad (21)$$

$$Q_x = b_1\cos^2\alpha + b_2\cos\alpha + b_3, \quad (22)$$

where a_1, a_2, a_3, b_1, b_2, and b_3 are the fitted coefficients. Extensive tabulations of these coefficients, for 27 elements and 396 photoelectron lines, are available in the literature.[14] Seah and Gilmore[19] proposed the following expression for Q_x:

$$Q_x = Q_x(0)(0.863 + 0.308\cos\alpha - 0.171\cos^2\alpha), \quad (23)$$

where $Q_x(0)$ is the value of Q_x for $\alpha = 0$.

$$Q_x(0) = 0.912 + 0.0148(Z+16.21)\exp[-(Z+16.21)/16.21] + (3.07\times10^{-5} - 2.09\times10^{-7}Z)(E-1200) - (7.75\times10^{-8} - 1.45\times10^{-9}Z)(E-1200)^2 \quad (E \text{ in eV}) \quad (24)$$

The expression for β_{eff} has a similar form,

$$\beta_{eff} = \beta_{eff}(0)(0.0868\cos^2\alpha - 0.208\cos\alpha + 1.121), \quad (25)$$

where $\beta_{eff}(0)$ is the value of β_{eff} for $\alpha = 0$.

$$\beta_{eff}(0)/\beta = 0.684 + 0.1005(Z+6.47)\exp[-(Z+6.47)/6.47] + (1.598\times10^{-4} - 5.567\times10^{-6}Z + 5.310\times10^{-8}Z^2)(E-1200). \quad (26)$$

The parameters $Q_x(0)$ and $\beta_{eff}(0)$ can also be expressed in terms of the single scattering albedo, ω:

$$Q_x(0) = (1-\omega)^{1/2}\left[0.091 + \frac{2.684}{1+1.908(1-\omega)^{1/2}}\right] \quad \text{for } \omega \geq 0.245, \quad (27a)$$

$$Q_x(0) = (1-\omega)^{1/2}(1+0.412\omega) \quad \text{for } \omega < 0.245, \quad (27b)$$

$$\beta_{eff}(0) = 0.876\beta[1 - \omega(0.955 - 0.0777\ln Z)]. \quad (28)$$

Equations (27) and (28) are considered to be more accurate than Eqs. (24) and (26).

Equations proposed by Seah and Gilmore[19] can in principle be generalized to compounds using the averaged atomic number (Eq. (20)). However, these authors recommended the following procedure for a given photoelectron line in a compound consisting of n elements:

$$Q_{compound} = \sum_{i=1}^{n} x_i[Q_x(\alpha)]_i, \quad (29a)$$

$$[\beta_{eff}/\beta]_{compound} = \sum_{i=1}^{n} x_i[\beta_{eff}(\alpha)/\beta]_i, \quad (29b)$$

where index i refers to pure elements. Equations (29a) and (29b) have obvious limitations in practical use. They cannot be applied to compounds in which one of the elements is gaseous, *e.g.* oxides or nitrides.

2·5 Separate expressions for the TMFP and the IMFP

The majority of predictive formulas for calculating the corrections Q_x and β_{eff} require knowledge of the single-scattering albedo, ω (or the ratio ζ). In principle, these parameters can be calculated using separate predictive expressions for the TMFP and the IMFP. This approach seems to be presently the most accurate, although it is rather tiresome for routine use. Let us

first address the algorithm for calculating the TMFP. Several expressions were published in the literature.[24-26] We describe below the most recent formalism.[26]

For compounds or alloys consisting of m elements, the TMFP is related to the transport cross sections (TCS) of atoms constituting a given solid,

$$\lambda_{tr} = \left(N \sum_{i=1}^{m} x_i \sigma_{tr,i} \right)^{-1}, \quad (30)$$

where $\sigma_{tr,i}$ is the TCS for the ith element, and N is the atomic density of a solid. For a given element, TCS can be calculated from an analytical expression consisting of two parts: (i) an analytical formula derived within the first Born approximation for the screened Rutherford potential, σ_{tr}^{B}, and (ii) a correcting function, $G(\varepsilon_0)$.

$$\sigma_{tr} = \sigma_{tr}^{B} G(\varepsilon_0), \quad (31)$$

where ε_0 is

$$\varepsilon_0 = \frac{8mc_F^2 a_0^2}{\hbar^2} \frac{E}{(\mu^\infty)^2 Z^{2/3}} = 0.230440 \frac{E}{(\mu^\infty)^2 Z^{2/3}}, \quad (32a)$$

$$c_F = \frac{1}{2}\left(\frac{3\pi}{4} \right)^{2/3} = 0.8853414, \quad (32b)$$

$$\sigma_{tr}^{B} = \frac{32\pi Z^{2/3} c_F^4 a_0^2}{(\mu^\infty)^4} \frac{1}{\varepsilon_0^2} \left[\ln(1+\varepsilon_0) - \frac{\varepsilon_0}{1+\varepsilon_0} \right], \quad (32c)$$

$$G(\varepsilon_0) = \varepsilon_0 \exp\left\{ \sum_{i=0}^{4} A_i \left[\ln(10\varepsilon_0) \right]^{i/2} \right\}, \quad (32d)$$

where A_i, $0 \le i \le 4$ are fitted coefficients. These coefficients are available for all elements, and for two energy ranges: from 50 to 300 eV, and from 300 eV to 30 keV.[26] It has been shown that the mean deviation between the accurate TCS and the TCS resulting from Eq. (31) varies between 0.01 and 0.5%, depending on element. Thus, the accuracy of the above formalism is rather high, between two and four decimal digits.

The TPP-2M predictive formula for calculating the IMFP has the form[23]

$$\lambda_{in} = \frac{E}{E_p^2 [\beta \ln(\gamma E) - (C/E) + (D/E^2)]}, \quad (33)$$

where E is the electron energy (in eV), and

$$E_p = 28.8 (N_v \rho / M)^{1/2} \quad (34a)$$

$$\beta = -0.10 + 0.944/(E_p^2 + E_g^2)^{1/2} + 0.069 \rho^{0.1}, \quad (34b)$$

$$\gamma = 0.191 \rho^{-0.50}, \quad (34c)$$

$$C = 1.97 - 0.91U, \quad (34d)$$

$$D = 53.4 - 20.8U, \quad (34e)$$

$$U = N_v \rho / M = E_p^2 / 829.4. \quad (34f)$$

In Eqs. (34a) - (34f), N_v is the number of valence electrons per atom or molecule, ρ the material density (in g/cm^3), M the atomic or molecular weight, and E_g the band-gap energy (in eV). The input parameters for calculating the IMFP from Eqs. (33) - (34) are: E, N_v, E_g and ρ. The recommended values of N_v for all elements are available in published tabulations.[27,28] These values can be used for estimating the N_v value for a given compound. The band-gap energy, E_g, for conductors is equal to zero. For other solids, some values are available in the literature. The rough guidance for estimating these values is published in a manual for the NIST IMFP database.[28] Fortunately, the IMFP is not a strong function of E_g, so a rough estimation is sufficient.

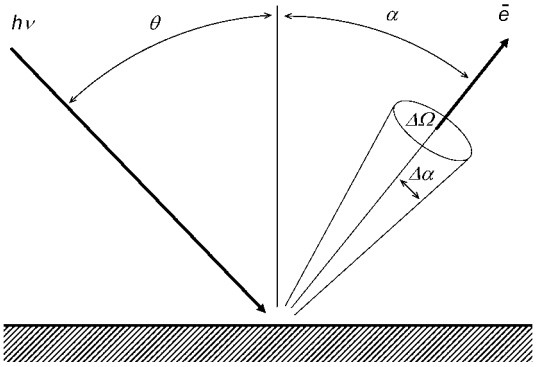

Fig. 2 Notation defining the XPS configuration. Note that the angle θ becomes negative if the direction of X-rays and the analyzer axis are located on the same side of the surface normal.

3 Master Angle Approach

The introduction of correction parameters for the elastic scattering effects into the formalism of quantitative XPS certainly complicates the computational procedure. First, we address here a question whether there are certain XPS configurations in which the elastic scattering effects are minimized.

We consider an experimental configuration in which the direction of X-rays, the analyzer axis and the surface normal are located in one plane (Fig. 2). Let us calculate the photoelectron signal intensity dependence on the incidence angle of X-rays, θ, for a constant emission angle, α. For this purpose, we use two theoretical models, one with the photoelectron elastic scattering neglected, and the second with the elastic scattering accounted for. On comparing of Eqs. (4) and (11), we can see that the signal intensity is proportional to the photoelectric cross section corrected for elastic-scattering effects, $(d\sigma_x/d\Omega)_{corr}$, or uncorrected for these effects, $(d\sigma_x/d\Omega)$. The corrected photoelectric cross section is calculated using the parameters Q_x and β_{eff} obtained from Eqs. (21) and (22) using fitted coefficients of Jablonski.[14] The results of calculations for Cu $2p_{3/2}$ photoelectrons are shown in Fig. 3. For some experimental geometries, the elastic scattering effects are significant. Figure 4 shows the ratio I_x^{el}/I_x^{nel} calculated for three photoelectron lines: Cu $2p_{3/2}$, Ag $3d_{5/2}$ and Au $4f_{7/2}$. As one can see, this ratio varies between 0.83 and 1.74. We note, however, that there are certain XPS configurations, defined by angles θ and α, in which the signal intensity is identical for both theoretical models. The angle between the direction of X-rays and the analyzer axis for such configurations has been tentatively termed the "Master Angle".[13] For the master angle, denoted by ψ_0, we have: $I_x^{nel} = I_x^{el}$ where the superscript "nel" denotes the common formalism. Consequently,

$$W(\beta, \psi_0) = Q_x W(\beta_{eff}, \psi_0) \quad (35)$$

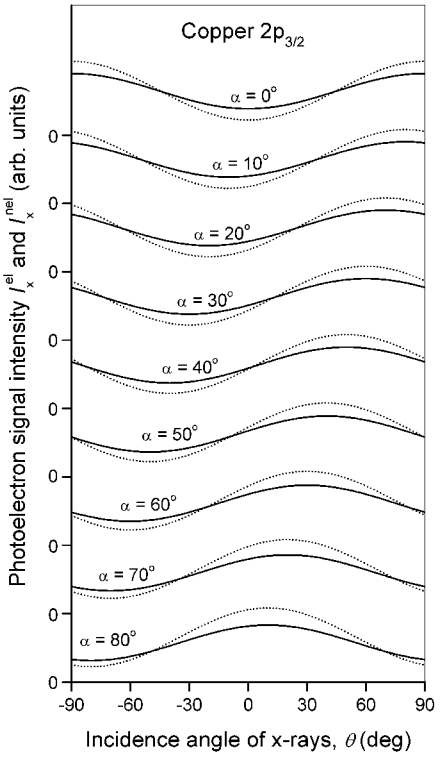

Fig. 3 Dependence of the photoelectron signal intensity on the incidence angle of X-rays, θ, calculated for Cu $2p_{3/2}$ photoelectrons for different emission angles, α (Al K_α radiation). Solid line, intensity I_x^{el} calculated from the model that takes into account the elastic photoelectron scattering; dotted line, intensity I_x^{nel} calculated from the common formalism neglecting elastic scattering. Ticks on the ordinate axis indicate zero positions for consecutive plots.

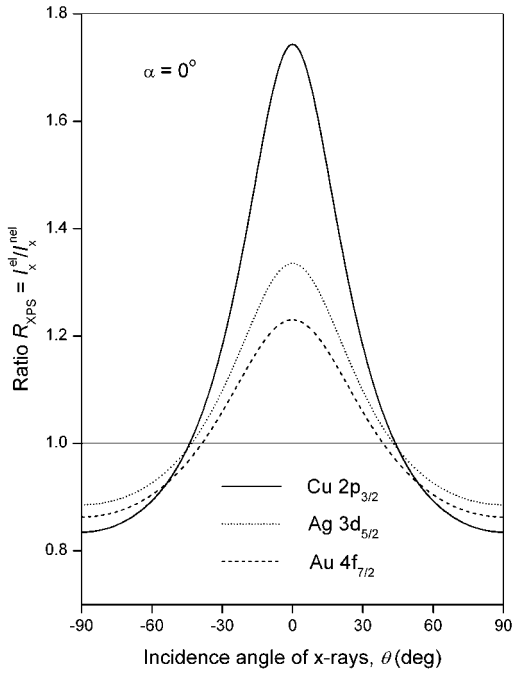

Fig. 4 Dependence of the ratio, $R_{XPS} = I_x^{el}/I_x^{nel}$, on the incidence angle of X-rays, θ. Solid line, Cu $2p_{3/2}$ photoelectrons; dotted line, Ag $3d_{5/2}$ photoelectrons; dashed line, Au $4f_{7/2}$ photoelectrons.

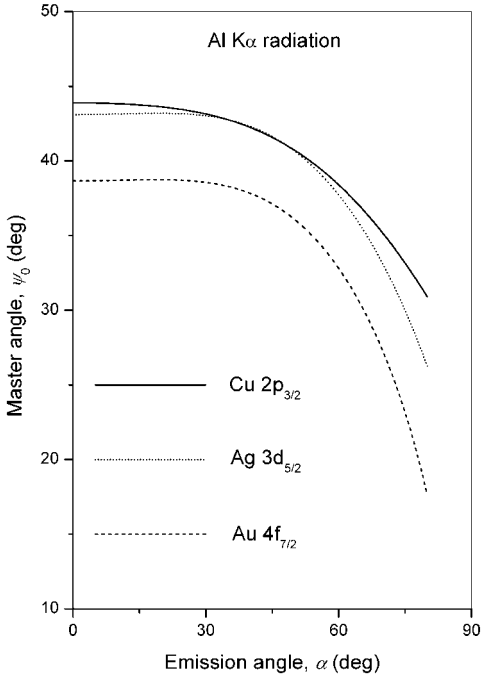

Fig. 5 Dependence of the master angle, ψ_0, on the photoelectron emission angle, α. Solid line, Cu $2p_{3/2}$ photoelectrons; dotted line, Ag $3d_{5/2}$ photoelectrons; dashed line, Au $4f_{7/2}$ photoelectrons.

and

$$\cos\psi_0 = \left[\frac{1}{3}\left(1+\frac{4(1-Q_x)}{\beta-\beta_{eff}Q_x}\right)\right]^{1/2}. \quad (36)$$

In contrast to the "Magic Angle" [$\psi_M = \arccos(3^{-1/2}) = 54^\circ 44' 8''$], the master angle is not a constant. Similarly as corrections Q_x and β_{eff}, the master angle depends on the photoelectron line, the emission angle of photoelectrons, and the solid. Figure 5 shows the emission angle dependence of the master angle for Cu $2p_{3/2}$, Ag $3d_{5/2}$ and Au $4f_{7/2}$ photoelectron lines calculated for the respective pure metals. In all cases, the master angle is considerably smaller than the magic angle. A similar observation was reported for different photoelectron lines in gold.[13]

If the master angles at a particular emission angle are identical for all photoelectron lines recorded for a given sample, then the simplest way to account for elastic scattering is to perform measurements in such a geometry. However, such a coincidence cannot be expected to be a rule. The master angle is frequently smaller than 40°, and the relevant configuration is not typical in XPS spectrometers. In general, we need to apply one of the correction procedures described in earlier sections.

4 Multiline Approach

In geometries in which large elastic scattering effects are found, we also expect that the surface composition calculated from the XPS formalism, in which the photoelectron elastic scattering is taken into account, differs noticeably from the composition calculated from the common formalism. The procedure of introducing corrections for photoelectron elastic scattering is demonstrated below for an example of procedure called multiline analysis.[29,30]

Let us consider a uniform sample consisting of n elements. Suppose that m_i photoelectron signal intensities were measured for the ith element. At least one photoelectron intensity is measured for an element present in the sample. Multiline analysis leads to surface composition, such that the calculated photoelectron intensities are closest to the measured intensities. We assume that the energy dependence of the IMFP for a given sample can be expressed by a simple relation resulting from the Bethe equation,

$$\lambda_{in} = h\frac{E}{\ln(\gamma E)} \tag{37}$$

where the coefficient h depends on a sample and the coefficient γ is constant for a wide class of materials. It has been found[31] that the latter coefficient is equal to 0.05359 for elements, 0.05046 for inorganic compounds, and 0.09554 for organic compounds. This coefficient averaged over all solids is equal to 0.06403.

Let us denote by I_i^k the kth photoelectron intensity due to the ith element. We have

$$I_i^k = TD_eA_0F_x\Delta\Omega h\frac{E_i^k}{\ln(\gamma E_i^k)}(d\sigma_x/d\Omega)_i^k Mx_i, \tag{38}$$

where M is the total atomic density of the sample, and x_i is the atom fraction. Equation (38) may be rewritten as

$$I_i^k = CD_i^k x_i, \tag{39}$$

where

$$C = F_x\Delta\Omega Mh, \tag{40}$$

$$D_i^k = S(E_i^k)\frac{E_i^k}{\ln(\gamma E_i^k)}(d\sigma_x/d\Omega)_i^k = S(E_i^k)\frac{E_i^k}{\ln(\gamma E_i^k)}(\sigma_x)_i^k W(\beta_i^k,\psi). \tag{41}$$

The product $S(E) = TD_eA_0$ is the spectrometer function associated with the properties of a given instrument. According to a multiline analysis model designated by MLA-2, the surface concentration of ith element is calculated from:[30]

$$x_i = \frac{y_i}{\sum_{i=1}^{n} y_i}, \tag{42}$$

where

$$y_i = \frac{\sum_{k=1}^{m_i}(I_i^k)^2 D_i^k}{\sum_{k=1}^{m_i} I_i^k (D_i^k)^2}. \tag{43}$$

Any algorithm for calculating the surface composition, taking into account elastic photoelectron scattering, becomes equivalent to solving a system of nonlinear equations. We look for concentrations that are initially unknown; however, to calculate the corrections Q_x and β_{eff}, we need to assume a certain composition. It has been found that the following iteration procedure is effective for correcting the multiline algorithm for elastic photoelectron collisions:

1. We calculate the surface composition using the uncorrected formalism (Eqs. (41) - (43)).

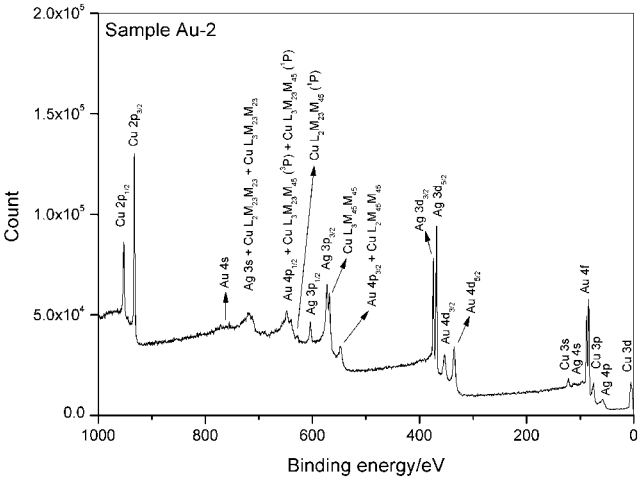

Fig. 6 Survey spectrum recorded for the Au-2 sample in the experimental configuration defined by angles $\theta = 45^\circ$ and $\alpha = 45^\circ$ (Al K_α radiation).

2. For current surface concentrations, x_i, we calculate the average atomic number.
3. From one of the described above algorithms, we calculate corrections Q_x and β_{eff} for all measured photoelectron lines.
4. We calculate the parameters, D_i^k (Eq. (41)) modified as follows:

$$D_i^k == S(E_i^k)\frac{E_i^k}{\ln(\gamma E_i^k)}(\sigma_x)_i^k(Q_x)_i^k W[(\beta_{eff})_i^k,\psi]. \tag{44}$$

5. We calculate a new surface composition from Eqs. (42) and (43).
6. If the surface composition is different from the initial composition, we return to step No. 2 and repeat the calculations.

Generally, the above iterations turn out to be quickly convergent.

5 Case Studies

In order to visualize the influence of photoelectron elastic scattering on the calculated composition, let us apply the described procedures of quantitative analysis to well-characterized samples. The samples used for that purpose were Certified Reference Materials for X-ray fluorescence spectrometry. They were manufactured and certified by Polish State Mint (Mennica, Metale Szlachetne). Two samples were submitted to analysis:

Au-2 sample: Au 33.35 ± 0.03 wt%, Ag 44.65 ± 0.05 wt%, and Cu 21.98 ± 0.05 wt%,

Au-6 sample: Au 49.99 ± 0.07 wt%, Ag 12.54 ± 0.05 wt%, Cu12.53 ± 0.05 wt%, and Pd 24.96 ± 0.04 wt%.

The alloys were prepared in the form of a thin foil, the thickness of which was close to 100 μm deposited on an aluminium alloy support with a diameter of 30 mm.

The XPS spectra were recorded using a PHI 5000 VersaProbe™ spectrometer with monochromatic Al K_α radiation. The X-ray beam was incident at the surface at $\theta = 45^\circ$ with respect to the surface normal. The analyzer axis was located at $\alpha = 45^\circ$ with respect to the surface normal. Consequently, the angle ψ was equal to 90°. For high-resolution spectra, the analyzer pass energy was 23.5 eV and the energy step size was 0.1 eV.

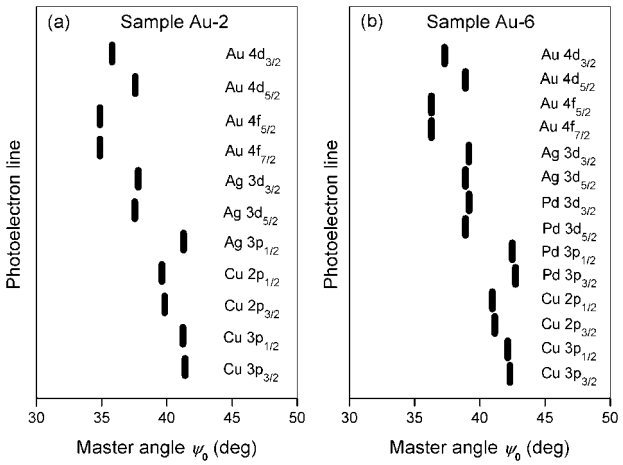

Fig. 7 Master angle values calculated for photoelectron lines recorded for the studied alloys. The bulk composition was assumed in calculations. (a) Alloy Au-2; (b) alloy Au-6.

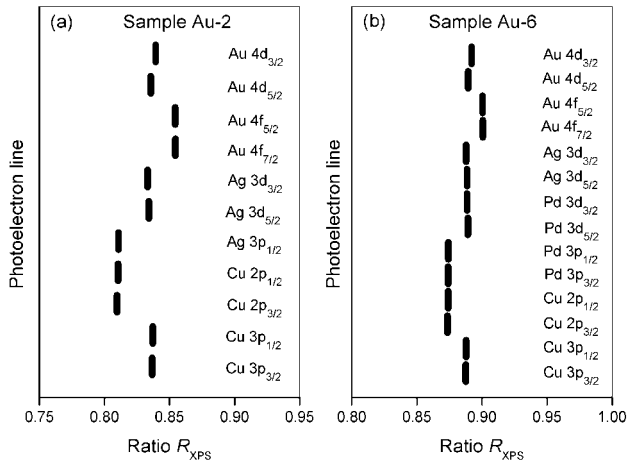

Fig. 8 The ratios R_{XPS} calculated for photoelectron lines recorded for the studied alloys. The bulk composition was assumed in calculations. (a) Alloy Au-2; (b) alloy Au-6.

The analyzer pass energy was 117.4 eV and the energy step size was 0.4 eV for recording the survey spectra. Prior to an XPS analysis, a sample area of 2 by 2 mm was cleaned for 2 min by argon ion sputtering. Ar^+ ions of energy 3 kV were incident at an angle of 55° with respect to the surface normal. After the cleaning procedure, the peaks due to contamination (carbon and oxygen) were no longer visible in the spectra. An exemplary survey spectrum for the Au-2 sample is shown in Fig. 6.

5·1 Master angles for studied alloys

From a spectrum recorded for the Au-2 sample, eleven photoelectron lines were selected for quantitative analysis and integrated (Cu $3p_{3/2}$, Cu $3p_{1/2}$, Cu $2p_{3/2}$, Cu $2p_{1/2}$, Ag $3p_{1/2}$, Ag $3d_{5/2}$, Ag $3d_{3/2}$, Au $4f_{7/2}$, Au $4f_{5/2}$, Au $4d_{5/2}$ and Au $4d_{3/2}$). For the Au-6 sample, fourteen photoelectron lines were integrated (Cu $3p_{3/2}$, Cu $3p_{1/2}$, Cu $2p_{3/2}$, Cu $2p_{1/2}$, Pd $3p_{3/2}$, Pd $3p_{1/2}$, Pd $3d_{5/2}$, Pd $3d_{3/2}$, Ag $3d_{5/2}$, Ag $3d_{3/2}$, Au $4f_{7/2}$, Au $4f_{5/2}$, Au $4d_{5/2}$ and Au $4d_{3/2}$). XPS spectra processing (background subtraction, peak fitting, integration) was performed using the software Avantage, version 4.30 (Thermo Fisher Scientific). The master angles were calculated from Eq. (36) using the corrections Q_x and β_{eff} determined for a given alloy assuming bulk composition. An algorithm of Jablonski and Powell[18] was used in calculations of the ratios, ζ. The average atomic number was estimated from Eq. (20), and the needed coefficients, Γ_k, were taken from Ref. 18. The results of calculations are listed in Fig. 7. For the Au-2 alloy (Fig. 7(a)), the master angles were contained in a relatively narrow angular range, from 34.78° to 41.40°. If an XPS analysis could be made in a configuration determined by ψ_0 equal to an intermediate angle (*e.g.* the value of 38.13° in the middle of angular range), we may expect that the elastic-scattering effects would be minimal. Unfortunately, such a geometry is not available in typical spectrometers.

Similar results were obtained for the alloy Au-6 (Fig. 7(b)). The master angles varied from 36.29° to 42.70°. The value in the middle of that range ($\psi_0 = 39.5°$) was very close to that obtained for the Au-2 alloy.

5·2 A measure for elastic scattering effects

The angle ψ for the PHI 5000 VersaProbe TM spectrometer used in measurements reported here is equal to 90°, and thus the influence of elastic photoelectron scattering on the signal intensity is non-negligible. As a simple measure of this influence, we can tentatively propose the ratio $R_{XPS} = I_x^{el}/I_x^{nel}$. One can see in Fig. 4 that the elastic photoelectron collisions in the geometry of the measurements decrease the photoelectron intensity, and the decrease is the largest. For the selected three photoelectron lines, the ratio R_{XPS} varies between 0.835 and 0.886. These values refer to pure elements. Let us now calculate the ratios R_{XPS} for the analyzed alloys, assuming the bulk composition. Results obtained using the algorithm of Jablonski and Powell[18] for calculating I_x^{el} are shown in Fig. 8. For the Au-2 alloy, the ratio varies between 0.810 and 0.854, while for the Au-6 alloy it ranges from 0.874 to 0.901. The decrease in the photoelectron intensity due to elastic photoelectron collisions is significant in all cases. Note, however, that the decrease in the photoelectron intensity is very similar for all considered photoelectron lines, particularly for the Au-6 alloy (Fig. 8(b)). This is an important observation. If the photoelectron intensities vary by the same factor, then the surface concentrations calculated from any method involving relative sensitivity factors do not change. We may thus expect that the elastic photoelectron collisions only slightly affect the calculated concentrations of elements in the studied alloys.

5·3 Calculated surface composition

Two groups of photoelectron intensities were selected for calculations of the surface composition. In usual practice, we select the most pronounced line for each element. For the Au-2 alloy, as follows from Fig. 6, the Cu $2p_{3/2}$, Ag $3d_{5/2}$ and Au $4f_{7/2}$ lines are the most intense. Similarly, for the Au-6 alloy, we select the Cu $2p_{3/2}$, Pd $3d_{5/2}$, Ag $3d_{5/2}$ and Au $4f_{7/2}$ photoelectron lines. In the second group, all of the measured photoelectron lines were included.

The surface composition was calculated from a multiline approach. The concentrations of elements were calculated from an uncorrected formalism (Eqs. (41) - (43)), and also from the described iteration procedure to take into account the elastic photoelectron collisions. Parameters Q_x and β_{eff} were calculated from the algorithm of Jablonski[17] and from the algorithm of Jablonski and Powell.[18] Results of calculations are listed in Tables 1 and 2.

Several conclusions follow from these data. First, according to expectations, the surface concentrations are only slightly

Table 1 Surface composition of the reference alloy Au-2 obtained from the multiline algorithm

Method	Composition (mass fraction)		
	Cu	Ag	Au
Three most pronounced photoelectron lines: Cu $2p_{3/2}$, Ag $3d_{5/2}$ and Au $4f_{7/2}$			
Elastic scattering neglected	0.250	0.347	0.403
Elastic scattering accounted Algorithm of Jablonski[17]	0.258	0.348	0.394
Elastic scattering accounted Algorithm of Jablonski and Powell[18]	0.258	0.348	0.394
Eleven photoelectron lines			
Elastic scattering neglected	0.263	0.358	0.379
Elastic scattering accounted Algorithm of Jablonski1[7]	0.270	0.357	0.373
Elastic scattering accounted Algorithm of Jablonski and Powell[18]	0.270	0.357	0.373
Bulk composition	0.2198	0.4465	0.3335

Table 2 Surface composition of the reference alloy Au-6 obtained from the multiline algorithm

Algorithm	Composition (mass fraction)			
	Cu	Pd	Ag	Au
Four most pronounced photoelectron lines: Cu $2p_{3/2}$, Pd $3d_{5/2}$, Ag $3d_{5/2}$ and Au $4f_{7/2}$				
Elastic scattering neglected	0.114	0.276	0.084	0.526
Elastic scattering accounted Algorithm of Jablonski[17]	0.117	0.279	0.085	0.519
Elastic scattering accounted Algorithm of Jablonski and Powell[18]	0.116	0.278	0.085	0.522
Fourteen photoelectron lines				
Elastic scattering neglected	0.129	0.289	0.096	0.486
Elastic scattering accounted Algorithm of Jablonski[17]	0.131	0.292	0.096	0.481
Elastic scattering accounted Algorithm of Jablonski and Powell[18]	0.131	0.291	0.096	0.483
Bulk composition	0.1253	0.2496	0.1254	0.4999

varied when the elastic scattering effects are taken into account. The largest percentage variation was observed for copper in the Au-2 alloy. The mass fraction changed from 0.250 (uncorrected formalism) to 0.258 (formalism corrected for elastic scattering), *i.e.* by 3.1%. For other elements the percentage changes were even smaller. Second, both algorithms used for correcting for elastic scattering effects provided the same results. Finally, the surface composition in all cases differed from the bulk composition, although the difference for the Au-6 alloy was not pronounced. In fact, this difference is comparable to differences resulting from different groups of photoelectron intensities used in calculations. The discrepancy between the bulk and surface concentration can be partially ascribed to selective sputtering; however, this effect is not analyzed here. One should also stress the fact that the calculated surface composition generally depends on the photoelectron lines selected for analysis. We may expect that results obtained from calculations, in which all of the photoelectron lines were selected, are the most accurate.

6 Summary and Outlook

It should be mentioned here that the parameter R_{XPS} proposed as a measure of the elastic-scattering effects is closely related to the effective attenuation length (EAL) for determining the surface composition. EAL is defined as a "parameter which, when introduced in place of the IMFP into an expression derived for AES and XPS on the assumption that elastic-scattering effects are negligible for a given quantitative application, will correct that expression for elastic scattering effects".[32] We have

$$R_{XPS} = I_x^{el}/I_x^{nel} = \frac{\lambda_{in} Q_x W(\beta_{eff}, \psi) / W(\beta, \psi)}{\lambda_{in}} = \frac{L_{QA}}{\lambda_{in}}, \quad (45)$$

where L_{QA} is the EAL for quantitative analysis. We can see that L_{QA} approaches the IMFP when the elastic scattering effects are neglected.

As follows from Fig. 4, the largest percentage deviations between the photoelectron intensities, calculated from the common formalism and from a model taking into account the elastic-scattering effects, are expected for angles ψ smaller than 30°, especially in the region of ψ angles close to zero. Furthermore, for such geometries, the elastic scattering effects strongly depend on the photoelectron line. However, this is not a typical experimental configuration. There are only a few reports in which such a configuration was used.[33-35] It is obvious that, in such a configuration, the use of a formalism taking into account the elastic scattering effects is crucial.

Jablonski and Zemek[35] compiled the master angles for 396 photoelectron lines in 27 solids. They found that the master angles for different subshells are grouped in relatively narrow ranges. For example, the master angles for photoelectrons emitted from the f-subshells typically range from 36° to 40°. If the photoelectron lines in a studied solid have master angles in a relatively small range, then measurements in such a geometry may be recommended. Unfortunately, special constructions of spectrometers are needed for these measurements, for example spectrometers with a rotatable analyzer. When the sample is in the form of a thin foil, the preferable configuration would be such that the X-ray source and the analyzer are located on opposite sides of the foil.

In a typical XPS configuration, in which the angle ψ is equal to, or exceeds, the magic angle, some caution is advisable. Results presented here refer to two specific alloys only for which the elastic scattering effects are similar at $\psi = 90°$. In general, the conclusions presented here may not be valid, and, for safety, it would be useful to check the influence of elastic scattering. As a guidance, we can use the algorithms presented here while assuming in calculations the bulk composition or the composition resulting from the formalism which neglected elastic scattering effects. It seems, however, that this is a fairly frequent occurrence that the decrease in the signal intensity due to elastic photoelectron collisions is comparable for the photoelectron lines recorded for a given sample. In consequence, a quantitative analysis of the surface composition by XPS, based on the typically used formalism, neglecting elastic scattering, is considered to be a very reliable technique.

On the other hand, we may encounter a situation in which one of the lines is affected more strongly by elastic scattering (*e.g.* due to distinctly different kinetic energy). Thus, the software packages for calculating the surface composition should have an option of including corrections for elastic scattering in

calculations of the surface composition. Such an extension is presently designed in the software package MULTI, implementing the multiline approach.[30,36] More effort should also be put to derive accurate and easy-to-use predictive formulas for the parameters Q_x and β_{eff}. Work on this problem is now in progress.[37] Finally, attention should be drawn to the fact that the reference database of parameters Q_x and β_{eff} was calculated using the elastic-scattering cross sections calculated for the Thomas–Fermi–Dirac potential.[14] It is now known that the cross sections calculated for the Dirac–Hartree–Fock potential are more accurate.[38] Thus, it would be useful to recalculate the reference data on Q_x and β_{eff} from a formalism that takes into account recent progress in the theory of electron transport. This work is planned for the near future.

7 Acknowledgements

The author would like to thank Dr W. Lisowski for performing the XPS measurements.

8 References

1. C. J. Powell and A. Jablonski, *Nucl. Instrum. Methods Phys. Res., Sect. A*, **2009**, *601*, 54.
2. C. S. Fadley, R. J. Baird, W. Siekhaus, T. Novakov, and S. A. L. Bergstrom, *J. Electron Spectrosc. Relat. Phenom.* **1974**, *4*, 93.
3. I. S. Tilinin, A. Jablonski, and W. S. M. Werner, *Prog. Surf. Sci*., **1996**, *52*, 193.
4. W. S. M. Werner, *Surf. Interface Anal*., **2001**, *31*, 141.
5. D. Briggs and M. P. Seah (ed.), "*Practical Surface Analysis: Auger and X-ray Photoelectron Spectroscopy*", 2nd ed., **1990**, Vol. 1, Chap. 5, Wiley, Chichester.
6. D. Briggs and J. T. Grant (ed.), "*Surface Analysis by Auger and X-ray Photoelectron Spectroscopy*", **2003**, IM Publishers, Chichester.
7. P. J. Feibelman, *Phys. Rev. B*, **1973**, *7*, 2305.
8. O. A. Baschenko and V. I. Nefedov, *J. Electron Spectrosc. Relat. Phenom*., **1979**, *17*, 405.
9. O. A. Baschenko and V. I. Nefedov, *J. Electron Spectrosc. Relat. Phenom*., **1980**, *21*, 153.
10. O. A. Baschenko and V. I. Nefedov, *J. Electron Spectrosc. Relat. Phenom*., **1982**, *27*, 109.
11. A. Jablonski, *Surf. Interface Anal*., **1989**, *14*, 659.
12. C. J. Powell and A. Jablonski, *J. Electron Spectrosc. Relat. Phenom*., **2010**, in press.
13. A. Jablonski and C. J. Powell, *Phys. Rev. B*, **1994**, *50*, 4739.
14. A. Jablonski, *Surf. Interface Anal*., **1995**, *23*, 29.
15. C. J. Powell and A. Jablonski, NIST Electron Effective-Attenuation-Length Database Ver. 1.1, Standard Reference Data Program Database 82, US Department of Commerce, **2003**, National Institute of Standards and Technology, Gaithersburg, MD, http://www.nist.gov/srd/nist82.htm.
16. A. Jablonski and I. S. Tilinin, *J. Electron Spectrosc. Relat. Phenom*., **1995**, *74*, 207.
17. A. Jablonski, *Surf. Sci*., **1996**, *364*, 380.
18. A. Jablonski and C. J. Powell, *J. Vac. Sci. Technol., A*. **1997**, *15*, 2095.
19. M. P. Seah and I. S. Gilmore, *Surf. Interface Anal*., **2001**, *31*, 835.
20. S. Chandrasekhar, "*Radiative Transfer*", **1960**, Chap. 5, Dover Publications, New York.
21. C. J. Powell and A. Jablonski, *J. Phys. Chem. Ref. Data*, **1999**, *28*, 19.
22. S. Tanuma, C. J. Powell, and D. R. Penn, *Surf. Interface Anal*., **1991**, *17*, 911.
23. S. Tanuma, C. J. Powell, and D. R. Penn, *Surf. Interface Anal*., **1994**, *21*, 165.
24. I. S. Tilinin, *Phys. Rev. A*, **1995**, *51*, 3058.
25. A. Jablonski, *Phys. Rev. B*, **1998**, *58*, 16470.
26. A. Jablonski and C. J. Powell, *Phys. Rev. B*, **2007**, *76*, 085123.
27. S. Tanuma, C. J. Powell, and D. R. Penn, *Surf. Interface Anal*., **2003**, *35*, 268.
28. C. J. Powell and A. Jablonski, NIST Electron Inelastic-Mean-Free-Path Database, Version 1.1, Standard Reference Data Program Database 71, U.S. Department of Commerce, **2000**, National Institute of Standards and Technology, Gaithersburg, MD, http://www.nist.gov/srd/nist71.htm.
29. W. Hanke, H. Ebel, M. F. Ebel, A. Jablonski, and K. Hirokawa, *J. Electron Spectrosc. Relat. Phenom*., **1986**, *40*, 241.
30. A. Jablonski, B. Lesiak, L. Zommer, M. F. Ebel, H. Ebel, Y. Fukuda, Y. Suzuki, and S. Tougaard, *Surf. Interface Anal*., **1994**, *21*, 724.
31. A. Jablonski, *Surf. Interface Anal*., **1993**, *20*, 317.
32. ISO 18115, Surface Chemical Analysis—Vocabulary, **2001**, International Organisation for Standardisation, Geneva; ISO 18115, Surface Chemical Analysis—Vocabulary—Amendment 2, **2007**, International Organisation for Standardisation, Geneva.
33. O. A. Baschenko, G. V. Machavariani, and V. I. Nefedov, *J. Electron Spectrosc. Relat. Phenom*., **1984**, *34*, 305.
34. A. Jablonski and J. Zemek, *Phys. Rev. B*, **1993**, *48*, 4799.
35. A. Jablonski and J. Zemek, *Surf. Sci*., **1997**, *387*, 288.
36. For more information, contact A. Jablonski, Institute of Physical Chemistry, Warsaw, Poland, e-mail: jablo@ichf.edu.pl.
37. A. Jablonski and C. J. Powell, *Surf. Sci*., **2010**, in press.
38. A. Jablonski, F. Salvat, and C. J. Powell, *J. Phys. Chem. Ref. Data*, **2004**, *33*, 409.